Nanoscale

Accepted Manuscript

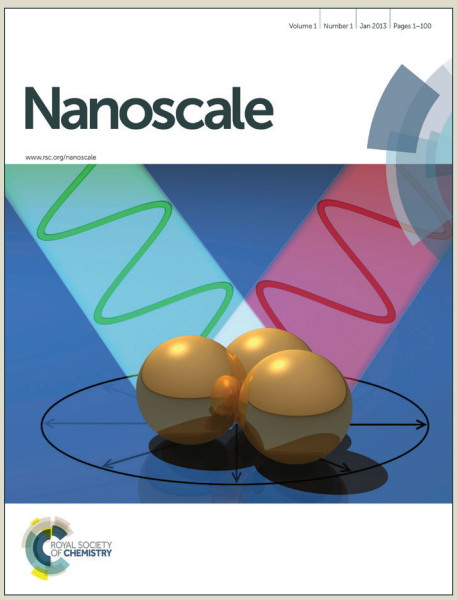

ROYAL SOCIETY OF CHEMISTRY

www.rsc.org/nanoscale

Journal Name

RSCPublishing

ARTICLE

Synthesis of chestnut-bur-like palladium nanostructures and their enhanced electrocatalytic activities for ethanol oxidation

Cite this: DOI: 10.1039/x0xx00000x

Seong Ji Ye,‡[a] Do Youb Kim,‡[b] Shin Wook Kang,[c,d] Kyeong Woo Choi,[a] Sang Woo Han,[c,d] and O Ok Park*[a]

Received 00th January 2012,
Accepted 00th January 2012

DOI: 10.1039/x0xx00000x

www.rsc.org/

We report a facile method for the synthesis of Pd nanostructures with highly open structure and huge surface area by reducing Na_2PdCl_4 with ascorbic acid and using cetylpyridinium chloride (CPC) as a surfactant in an aqueous solution. The prepared Pd nanostructures had an average overall size of 70 nm and were composed of dozens of needle-like thin arms, originating from the same core, with an average thickness of 2.3 nm; the arms looked like chestnut-burs. Time evolution of Pd nanostructures implied that small Pd particles generated at the early stage of the reaction by fast reduction grew *via* particle attachment growth mechanism. The morphology and size of the Pd nanostructures could be readily controlled by varying the concentration of CPC; depending on the amount of CPC, the reduction rates varied the morphology of the Pd nanostructures. Because of the huge surface area and possible catalytically active sites, the prepared chestnut-bur-like Pd nanostructures exhibited greater electrocatalytic activity toward ethanol electrooxidation compared to other Pd nanocatalysts, including cubic and octahedral Pd nanocrystals, and even commercial Pd/C.

Introduction

Research on the size and shape control of noble-metal nanocrystals has received a great deal of attention over the past decade. Because of their finely tunable physical and chemical properties achieved by controlling their shapes and sizes,[1] they can be applied to various fields such as catalysis,[2] medicine,[3] sensing,[4] imaging,[5] electronics,[6] and plasmonics.[7] Like other noble metals, Pd nanocrystals have attracted research interest because of their specific properties such as catalytic activity,[2b,8] hydrogen storage,[9] sensing,[10] and surface plasmon resonance (SPR),[11] which can be easily tuned by controlling their shapes and sizes. Moreover, the superior properties of Pd play very important roles in many industrial applications. Pd nanocrystals are especially valuable as catalysts for many chemical reactions; for example, as an electrocatalyst in fuel cells;[8a,12] as a catalyst for low-temperature reduction of automobile pollutants;[13] and as a catalyst for carbon–carbon bond formation reactions such as Suzuki, Heck, Stille coupling reactions.[8b,12b,14]

Among the various reactions of noble metals, Pd has been considered an attractive replacement of Pt as an electrocatalyst in fuel cells. Generally, Pt is used as an electrocatalyst for both hydrogen oxidation and oxygen reduction in fuel cells because of its high electrocatalytic activity. However, its use as a catalyst is restricted by its high cost and limited material availability. On the other hand, Pd shows the highest electrocatalytic activity in pure metals aside from Pt and is more abundantly available and has lower cost than Pt.[15] In addition, Pd-based catalysts exhibit higher electrocatalytic activities compared to Pt-based catalysts in some chemical reactions. This is especially true in alkaline-type direct alcohol fuel cells (DAFCs).[16] Therefore, many research groups have made great efforts to prepare Pd nanostructures with enhanced electrocatalytic activities by controlling their shapes and sizes.[2b,8a,12b,17]

Among the various morphologies of metal nanocrystals, highly branched morphologies have received particular interest for improving catalytic activities. Generally, metal nanostructures with highly branched structures possess large surface areas where catalytic reactions occur and also have a higher possibility of catalytically active sites such as corners, edges, and stepped atom planes within their branches.[18] There have been several reports of highly branched metal nanostructures with enhanced catalytic activities in several reactions, which include monometallic Pt[14b,18b,19] and Pd[14b,20] and bimetallic Au-Pd[21] and Pd-Pt[22] nanostructures. In the case of highly branched Pd nanostructures, Bao *et al.* demonstrated

the synthesis of porous Pd nanoflowers by a polyol process in the presence of oleylamine, *o*-dichlorobenzene, and 1,2-hexadecanediol at ~180 °C.[20a] The porous Pd nanoflowers showed higher electrocatalytic activity toward methanol oxidation in alkaline media compared to Pd nanoparticles. Remita *et al.* also reported on the synthesis of urchin-like Pd nanostructures by radiolytic reduction in the presence of cetylpyridinium chloride (CPC).[23] Han *et al.* demonstrated the synthesis of Pd nanodendrites using ascorbic acid as a reducing agent in the presence of cetyltrimetylammonium bromide (CTAB).[24] They also controlled the morphology of Pd nanocrystals by changing the reaction sequence.

Recently, our group reported morphology-controlled synthesis of flower-like Au@Pd nanostructures with branched morphologies using CPC as a surfactant.[25] Flower-like Au@Pd nanostructures can be obtained with the help of relatively long alkyl chains and rigid pyridinium groups of CPC. The morphology of these structures can be controlled by changing the amount of CPC in the reaction. Although the flower-like Au@Pd nanostructures showed enhanced electrocatalytic activity toward ethanol electrooxidation compared with the cuboctahedral Au@Pd nanostructures, the activity was still less than that of porous Pd structures,[26] in spite of Au@Pd nanostructures having costly Au in their cores. As an extension of these results, in this study, we report the synthesis of monometallic Pd nanostructures with highly branched, and thus highly open, structures. The highly branched Pd nanostructures were prepared by reducing Na_2PdCl_4 with ascorbic acid using CPC as a surfactant at 80 °C. The prepared Pd nanostructures had dozens of needle-like arms, originating from the core, with average thickness of only 2.3 nm. It is especially notable that these chestnut-bur-like Pd nanostructures were routinely prepared in aqueous solution using a facile, rapid (<7 min), one-pot synthesis with high yield without any preformed seeds. Moreover, the thickness of the arms could be readily controlled by changing the concentration of CPC. We also systemically investigated the formation mechanism of the chestnut-bur-like Pd nanostructures by observing the time evolution of the Pd nanostructures. Finally, morphology-dependent electrocatalytic activities of the Pd nanostructures toward ethanol electrooxidation were investigated using four different Pd nanocatalysts: chestnut-bur-like Pd nanostructures, Pd nanocubes, Pd nanooctahedra, and commercially available Pd/C. Our results showed that the chestnut-bur-like Pd nanostructures exhibited higher electrocatalytic activity than the Pd nanopolydedrons, and even the Pd/C catalyst.

Experimental

Chemicals and materials

Sodium tetrachloropalladate(II) (Na_2PdCl_4, 99.995%), *L*-ascorbic acid (AA, >99%), CPC (≥99%), and Pd/C (Pd, 10 wt.% on activated carbon) were purchased from Sigma-Aldrich. Acetone (99.0%) was obtained from Samchun Chemicals. In all experiments, deionized water with a resistivity of 18.2 MΩ was used and obtained from a Pure Power water purification system (Human, Korea).

Synthesis of chestnut-bur-like palladium nanostructures

In a typical synthesis of chestnut-bur-like Pd nanostructures, 2 mL of AA (10 mM) aqueous solution was injected into a mixture of 0.1 mL Na_2PdCl_4 aqueous solution (5 mM), 0.01 mM CPC aqueous solution (0.01 M), and 3.89 mL deionized water in a 30 mL vial and heated to 80 °C in an oil bath with magnetic stir bar for 7 min. During the reaction, the color of the reaction solution changed from brownish yellow to light black. After reaction finished, the reaction solution was centrifuged at 14,000 rpm for 5 min. and washed with deionized water two times to remove the residual capping agent.

Characterization

Transmission electron microscopy (TEM) images of the product were collected using a JEM-3011 (JEOL) transmission electron microscope, operating at an accelerating voltage of 300 kV. High-resolution TEM (HRTEM) images were obtained using a JEM-ARM200F (JEOL) Cs-corrected scanning transmission electron microscope operated at an accelerating voltage of 200 kV. The TEM and HRTEM samples were prepared by dropping a few drops of a colloidal suspension in deionized water on 300-mesh carbon-coated copper grids and drying at room temperature. The X-ray diffraction (XRD) patterns were recorded using an X-ray diffractometer (D/MAX-2500, Rigaku) with Cu Kα (0.1542 nm) radiation. The XRD samples were prepared through repeated dropping and drying of a colloidal suspension in water onto a glass substrate. Before measuring the electrochemical properties, the concentrations of the four different Pd nanocrystal suspensions in water were determined using an inductively-coupled plasma atomic emission spectrometer (ICP-AES, OPTIMA 3300 DV).

Electrochemical measurement

Electrochemical measurements were performed using a conventional three-electrode cell connected to a potentiostat (600C, CH Instrument). In the conventional three-electrode cell setup, a Pd nanocrystal-loaded glassy carbon electrode (GCE), Ag/AgCl (saturated with KCl), and platinum wire were used as working, reference, and counter electrodes, respectively. To prepare the working electrodes, 1 μg of one of the four different Pd nanocrystal suspensions was loaded by drop-casting onto the GCE, which was already polished with alumina powder and washed with deionized water. The amount of solution loaded for each of the different Pd nanocrystal solutions was determined based on the ICP-AES results. After the Pd nanocrystal-loaded GCEs were dried, 4 μL of a Nafion solution (0.05%) was drop-casted and dried again. The modified GCEs were washed with deionized water and electrochemically cleaned by 50 potential cycles between -0.85 and 0.45 V at a scan rate of 50 mV s^{-1} in 0.1 M KOH aqueous solution to eliminate the remaining stabilizing agents on the Pd nanocrystal surface. All cyclic voltammetry (CV) measurements were performed at room temperature and the electrolyte solutions

were purged for approximately 1 h with high-purity N_2 gas before use.

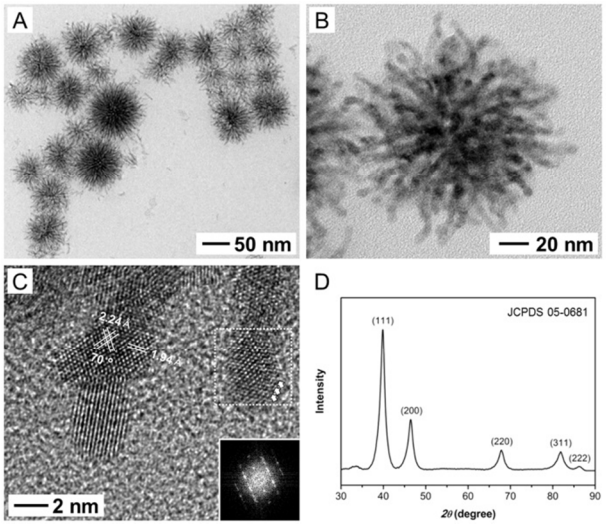

Fig. 1 Transmission electron microscopy (TEM) images of Pd nanostructures (A) and single Pd nanostructure (B) recorded at different magnifications. (C) High-resolution TEM (HRTEM) image taken from the apex of a single Pd nanostructure. Arrows indicate stacking faults and inset is the FFT pattern corresponding to the boxed area in the HRTEM image. (D) X-ray diffraction pattern of Pd nanostructures.

Results and Discussion

The chestnut-bur-like Pd nanostructures with highly branched structures were prepared by a facile, rapid, one-pot synthesis method in an aqueous reaction system. Briefly, chestnut-bur-like Pd nanostructures were obtained by the reduction of Na_2PdCl_4 (0.083 mM) with AA (3.33 mM) in the presence of CPC (0.017 mM) at 80 °C for 7 min (detailed experimental procedure can be seen in the Experimental section). Fig. 1A and B show the typical TEM images of the prepared Pd nanostructures and a single Pd nanostructure at different magnifications, respectively. As shown in the TEM images, the obtained Pd nanostructures have a unique morphology with highly open structure that includes more than dozens of thread-like arms stretched outward from the center, similar to chestnut burs. The average diameter of the Pd nanostructures was approximately 70 nm and the average thickness of the needle-like arms was approximately 2.3 nm. An HRTEM image recorded at the apex of an individual Pd nanostructure in Fig. 1C showed that the Pd nanostructure is not single crystalline with several stacking faults. The HRTEM image also showed *d*-spacings of 2.24 Å (with dihedral angle of ~70°) and 1.94 Å, which could be indexed to the {111} and {200} reflections of Pd, respectively. The XRD pattern taken from the Pd nanostructures also shows five distinct peaks, which correspond to the (111), (200), (220), (311) and (222) reflections of *fcc* Pd structure (JCPDS 05-0681) (Fig. 1D).

Because the chestnut-bur-like Pd nanostructures were polycrystalline, we hypothesized that the Pd nanostructures were grown by the particle attachment growth mechanism,[18a,22a] where small particles generated at the early stage of the reaction would coalesce into seeds, and the remaining small particles would be attached to the seeds in order to reduce the surface energy. In order to evaluate the growth mechanism of the chestnut-bur-like Pd nanostructures, the time evolution of the Pd nanostructures was observed by quenching the reaction at certain reaction times using precooled acetone. Fig. 2 shows the TEM images of Pd nanostructures obtained at different reaction times, showing the time evolution of the Pd nanostructures. When the reaction proceeded for a few seconds (~3 s), small Pd agglomerates (Fig. S1A in the ESI†) and Pd nanostructures looked like the initial states of the chestnut-bur-like Pd nanostructures (Fig. S1B in the ESI†), were observed as shown in Fig. 2A. In our experimental system, the reaction was relatively fast and as soon as the AA solution was injected into the reaction mixture at 80 °C, the reaction solution turned light black instantaneously, indicating the formation of Pd nanostructures. As the reaction progressed, the particles that appeared as the initial states of the chestnut-bur-like Pd nanostructures gradually developed their arms to form the final chestnut-bur-like morphology (Fig. 2B and 2C); after 7 min, no subsequent changes in their sizes and shapes were observed (Fig. 1A and Fig. 2D). On the other hand, the number of small Pd agglomerates steadily decreased as the reaction proceeded and the small Pd nanoparticles were barely observable after 7 min. The time evolution TEM images also show that the chestnut-bur-like Pd nanostructures grew via particle attachment. Frequent stacking faults were observed in the HRTEM images of Pd nanostructures (Fig. 1C and Fig. S2 in the ESI†) and the fact that the diameter of the small Pd particles was nearly the same as that of the arm thickness in chestnut-

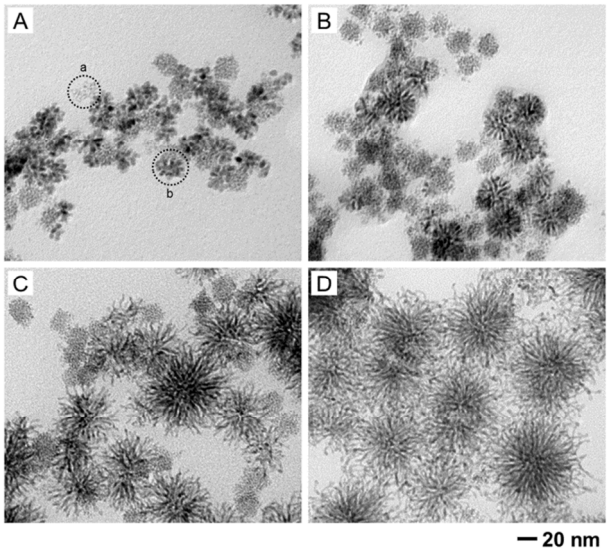

Fig. 2 Transmission electron microscopy (TEM) images of Pd nanostructures obtained under the same reaction conditions as those for Fig. 1 (the standard synthesis), except at different reaction times: (A) ~3 s, (B) 30 s, (C) 3 min, and (D) 10 min.

bur-like Pd nanostructures also supports the particle attachment growth mechanism of chestnut-bur-like Pd nanostructures.

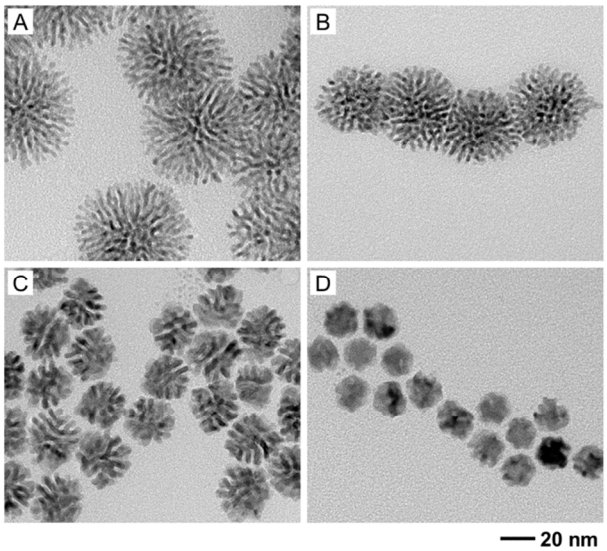

Fig. 3 Transmission electron microscopy (TEM) images of Pd nanostructures obtained using standard procedure but with different concentrations of cetylpyridinium chloride (CPC) in the reaction solution: (A) 0.167 mM, (B) 1.67 mM, (C) 33.0 mM, (D) 150 mM.

The morphology of the Pd nanostructures was easily controlled by varying the concentration of the CPC aqueous solution while keeping the other reaction conditions constant. Fig. 3 shows the TEM images of the Pd nanostructures synthesized by changing the concentration of the CPC aqueous solution. Note that the chestnut-bur-like Pd nanostructures with the thinnest arms (2.3 nm) observed were obtained under the standard synthesis conditions using 0.017 mM of CPC. When the concentration of CPC was <0.017 mM, the Pd nanostructures could not be effectively stabilized because of the insufficient amount of surfactant molecules, causing the Pd nanostructures to agglomerate and form larger irregular particles. In contrast, when the concentration of CPC was increased to 0.167 mM, chestnut-bur-like Pd nanostructures with smaller diameter (60.9 nm) and thicker arms (2.8 nm) were obtained (Fig. 3A), compared to the Pd nanostructures obtained by the standard procedure (Fig. 1). When the concentration of CPC was further increased to 1.67 and 33.0 mM, the diameter of Pd nanostructures was decreased to 48.3 and 28.0 nm and the thickness of the arms was increased to 3.1 and 4.0 nm, respectively (Fig. 3B and C). Chestnut-bur-like Pd nanostructures could not be obtained when the concentration of CPC was higher than 33.0 mM. As shown in Fig. 3D, when the concentration of CPC was 150 mM, spherical Pd nanostructures with rough surfaces and an average diameter of 18.9 nm were obtained.

The observed increases in the arm thickness of the Pd nanostructures based on the concentration of CPC were consistent with our previous report, according to which the morphology of flower-like Au@Pd nanostructures can be controlled by varying the concentration of CPC.[25] The morphological changes of the Pd nanostructures depending on the amount of CPC can be attributed to the different reduction rates of Pd. In the present reaction system, when a relatively small amount of CPC was used, the reduction rate was increased and relatively small Pd particles (known as seeds, <3 nm in diameter) were formed at a very early stage of the reaction. These small Pd seeds subsequently agglomerated and grew via attachment of the small remaining Pd seeds to form chestnut-bur-like Pd nanostructures (shown in Fig. 1). As the amount of CPC in the reaction system increased, the reduction rate was decreased and relatively larger Pd seeds (still <4 nm) were formed at an early stage of the reaction. These Pd seeds grew into chestnut-bur-like Pd nanostructures with thicker arms through the same growth mechanism (shown in Fig. 3A and B). However, when the amount of CPC was further increased, the growth of Pd nanostructures followed a conformal growth mechanism in addition to the particle attachment growth mechanism (shown in Fig. 3C and D). Because the reduction rate was considerably decreased, Pd ions were not totally consumed at the very early stages of the reaction. Some of Pd ions were consumed to generate small Pd seeds and these Pd seeds grew larger by attaching to one another in order to reduce the total surface energy. Meanwhile, the remaining Pd ions (including those from re-dissolved Pd nuclei, which were smaller than the critical size)[27] were gradually reduced and nucleated heterogeneously as the reaction progressed, which in turn led to conformal growth of Pd on the pre-formed Pd nanostructures. Comparing with our previous results on flower-like Au@Pd nanostructures, a much lower concentration of CPC was required in the current study to obtain chestnut-bur-like Pd nanostructures. In the case of the flower-like Au@Pd nanostructures, lower concentrations of CPC could not effectively stabilize the Au seed dispersion, which caused homogeneous Pd nucleation, away from the Au seed. Therefore, Pd grew from the Au seeds in an epitaxial manner.[25] This result supports our explanation of the morphological changes in the Pd nanostructures based on the concentration of CPC. The Pd polyhedrons obtained using a much larger amount of CPC (shown in Fig. S3 in the ESI†), where Pd nanostructures appeared to grow through nucleation and Ostwald ripening, also support our explanation.

The chestnut-bur-like Pd nanostructures are expected to provide a reasonably larger surface area compared to the Pd polyhedra because of their unique morphology with numerous needle-like arms, despite their relatively large overall size. In addition, metal nanocrystals with branched morphologies usually possess a higher density of catalytically active sites such as edges, corners, and atomic steps within the branches compared with particles with conventional morphologies, which leads to substantially enhanced catalytic activities.[18] In order to evaluate the electrocatalytic activity of the morphology-controlled Pd nanocrystals, we performed ethanol oxidation in alkaline solution as a probe reaction with four different nanocatalysts: chestnut-bur-like Pd nanostructures, Pd nanocubes, Pd nanooctahedra, and commercial Pd/C. The average edge length of Pd nanocubes and Pd nanooctahedra

were 14 ± 3 and 17 ± 3 nm, respectively (Fig. S4 in the ESI†). The total Pd loading amount on each glassy carbon electrode (GCE) was adjusted to 14.1 μg cm^{-2} for all samples.

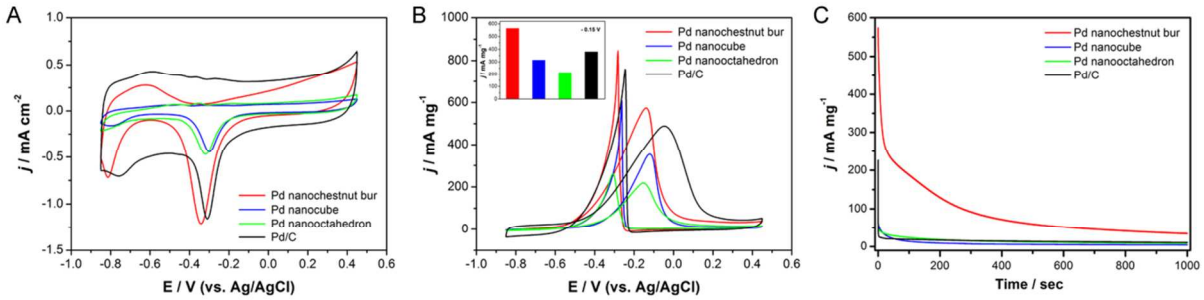

Fig. 4 Cyclic voltammetry (CV) curves of glassy carbon electrodes (GCEs) modified with four different Pd nanocatalysts in (A) 0.1 M KOH solution and (B) 0.1 M KOH + 0.1 M ethanol solution at a scan rate of 50 mV s^{-1}. Current densities were normalized with respect to (A) the geometric area of GCE (0.071 cm^2) and (B) the amount of Pd loading (1 μg) on the GCE. Inset in Fig. 4B shows mass activities of the four different Pd nanocatalysts at –0.15 V vs. Ag/AgCl.

Electrochemically active surface areas (ECSAs) for each of the four different Pd nanocatalysts on GCEs were obtained from cyclic voltamogramms in 0.1 M KOH solution (Fig. 4A). ECSA was calculated using the equation ECSA = Q_0/q_0, where Q_0 and q_0 represent the surface charge obtained from the area under the CV curves of palladium oxide reduction and charge required for the desorption of a monolayer of oxygen on the Pd surface (424 μC cm^{-2}), respectively.[28] Through this equation, ECSAs of chestnut-bur-like Pd nanostructures, Pd nanocubes, Pd nanooctahedra, and Pd/C were calculated to be 0.42, 0.16, 0.14, and 0.20 cm^2, respectively. Despite their relatively larger size, the ECSA of the chestnut-bur-like Pd nanostructures was larger than other three Pd nanocatalysts owing to their highly open structure. Fig. 4B shows the CVs of the four samples in 0.1 M KOH + 0.1 M ethanol, where the current densities were normalized with respect to the amount of Pd loading (1 μg). Although the Pd nanooctahedra showed the most negative oxidation potential at -0.15 V (vs. Ag/AgCl) among the four Pd nanocatalysts, the chestnut-bur-like Pd nanostructures also showed a relatively negative potential at -0.14 V (vs. Ag/AgCl) compared with the Pd nanocubes (-0.12 V vs. Ag/AgCl) and Pd/C (-0.05 V vs. Ag/AgCl). The CVs also clearly show that the mass activity of the chestnut-bur-like Pd nanostructures was greater than those of the Pd nanocubes, Pd nanoocatahedra, and even Pd/C (Fig. 4B). The mass activities of the four Pd nanocatalysts at -0.15 V (vs. Ag/AgCl) were 566.3 mA mg_{Pd}^{-1} for the chestnut-bur-like Pd nanostructures, 382.4 mA mg_{Pd}^{-1} for Pd/C, 316.9 mA mg_{Pd}^{-1} for the Pd nanocubes, and 217.6 mA mg_{Pd}^{-1} for the Pd nanooctahedra (Fig. 4B inset). The higher catalytic activity of the chestnut-bur-like Pd nanostructures toward ethanol oxidation could be attributed to their larger ECSA compared with the other Pd catalysts and additional possible catalytically active sites along the arms. In addition, the electrochemical stabilities of the four samples were also investigated by chroroamperometric measurement. Fig. 4C shows the curves of current densities *versus* time recorded at -0.2 V for 1000 s, indicating that the current density of the chestnut-bur-like Pd nanostructures was still higher than those of the other Pd structured catalysts after 1000 s. Taken together, these results indicate that the chestnut-bur-like Pd nanostructures have higher electrocatalytic activity and stability than the Pd nanocubes, Pd nanooctahedra, and even commercial Pd/C toward ethanol electrooxidation.

Comparing the electrocatalytic activity of the chestnut-bur-like Pd nanostructures with the previously reported Pd-based catalysts, electrocatalytic activity of the chestnut-bur-like Pd nanostructures was comparable or possibly higher than those toward ethanol electrooxidation. In a typical ethanol electrooxidation reaction in alkaline media, the current density is strongly influenced on the concentration of ethanol and alkaline media.[29] For example, as the concentration of ethanol is increased up to 4 M, while the concentration of alkaline media is kept the same, the current density also increases. On the other hand, when the concentration of ethanol is kept the same, the current density is increased as the concentration of the alkaline media is increased up to 1 M. However, further increase in the concentration of ethanol leads to decrease in the current density.[29] Likewise, we expect that the current density would increase when the concentration of ethanol and KOH are adjusted. Although the concentration of the alkaline media, KOH in this study, and ethanol were both relatively low as 0.1 M, the mass activity was comparable with the recently reported free-standing Pd-based membrane,[30] where 0.5 M of NaOH and 1 M ethanol were used for the measurement and Pd-Ni nanoalloys,[31] where 0.1 M KOH and 0.5 M ethanol were used.

Conclusion

In summary, we have demonstrated a rapid one-pot synthesis of chestnut-bur-like Pd nanostructures in high yields by reduction of Na_2PdCl_4 with ascorbic acid in the presence of CPC. Time evolution of Pd nanostructures indicated that small Pd nanoparticles nucleated at very early stages of the reaction and the growth proceeded via particle attachment. Furthermore, the morphology and size of the resultant Pd nanostructures could be easily controlled by varying the concentration of CPC solution added into the reaction system. The chestnut-bur-like Pd nanostructures exhibited greater electrocatalytic activity for

ethanol electrooxidation in an alkaline solution than the cubic and octahedral Pd nanocrystals, and even commercial Pd/C, owing to their larger ECSA and possible catalytically active sites. We expect that this synthetic strategy could be extended to the synthesis of metal nanostructures with highly branched morphology for highly active catalysts.

Acknowledgements

This research was supported by the Public Welfare & Safety Research Program through the National Research Foundation of Korea (NRF) funded by the Ministry of Science, ICT & Future Planning (MSIP) (2011-0028468). S.W.K. and S.W.H acknowledge the support from Institute for Basic Science (IBS) [CA1301].

Notes and references

[a] Department of Chemical and Biomolecular Engineering (BK21+ graduate program), Korea Advanced Institute of Science and Technology (KAIST), 291 Daehak-ro, Yuseong-gu, Daejeon 305-701, Republic of Korea.

[b] Advanced Materials Division, Korea Research Institute of Chemical Technology (KRICT), 141 Gajeong-ro, Yuseong-gu, Daejeon 305-600, Republic of Korea.

[c] Department of Chemistry and KI for the Nanocentry, Korea Advanced Institute of Science and Technology (KAIST), 291 Daehak-ro, Yuseong-gu, Daejeon 305-701, Republic of Korea.

[d] Center for Nanomaterials and Chemical Reactions, Institute for Basic Science (IBS), Daejeon 305-701, Republic of Korea.

‡ These authors contributed equally to this work.

† Electronic Supplementary Information (ESI) available: [Additional TEM images of Pd nanostructures (Fig. S1-S4)]. See DOI: 10.1039/b000000x/

1 a) Y. Xia, Y. Xiong, B. Lim, S. E. Skrabalak, *Angew. Chem. Int. Ed.*, 2009, **48**, 60; b) C. Burda, X. Chen, R. Narayanan, M. A. El-Sayed, *Chem. Rev.*, 2005, **105**, 1025.

2 a) J. Lee, S. E. Habas, S. Kweskin, D. Butcher, G. A. Somorjai, P. Yang, *Angew. Chem. Int. Ed.*, 2006, **45**, 7824; b) M. Jin, H. Zhang, Z. Xie, Y. Xia, *Energy Environ. Sci.*, 2012, **5**, 6352.

3 a) S. E. Skrabalak, J. Chen, L. Au, X. Lu, X. Li, Y. Xia, *Adv. Mater.*, 2007, **19**, 3177; b) Y.-H. Kim, J. Jeon, S. H. Hong, W.-K. Rhim, Y.-S. Lee, H. Youn, J.-K. Chung, M. C. Lee, D. S. Lee, K. W. Kang, J.-M. Nam, *Small*, 2011, **7**, 2052; c) P. Fortina, L. J. Kricka, D. J. Graves, J. Park, T. Hyslop, F. Tam, N. J. Halas, S. Surrey and S. A. Waldman, *Trends Biotechnol.*, 2007, **25**, 145.

4 a) P. Zhou, Z. Dai, M. Fang, X. Huang, J. Bao, J. Gong, *J. Phys. Chem. C*, 2007, **111**, 12609; b) X. Zhang, M. A. Young, O. Lyandres and R. P. Van Duyne, *J. Am. Chem. Soc.*, 2005, **127**, 4484.

5 a) X. Yang, S. E. Skrabalak, Z.-Y. Li, Y. Xia, L. V. Wang, *Nano Lett.*, 2007, **7**, 3798; b) D. Y. Kim, S. H. Im, O O. Park, Y. T. Lim, *CrystEngComm*, 2010, **12**, 116.

6 a) D. H. Wang, D. Y. Kim, K. W. Choi, J. H. Seo, S. H. Im, J. H. Park, O O. Park, A. J. Heeger, *Angew. Chem. Int. Ed.*, 2011, **50**, 5519; b) Y. Son, J. Yeo, H. Moon, T. W. Lim, S. Hong, K. H. Nam, S. Yoo, C. P. Grigoropoulos, D.-Y. Yang and S. H. Ko, *Adv. Mater.*, 2011, **23**, 3176.

7 a) M. B. Cortie, A. M. McDonagh, *Chem. Rev.*, 2011, **111**, 3713; b) S. A. Maier, M. L. Brongersma, P. G. Kik, S. Meltzer, A. A. G. Requicha, H. A. Atwater, *Adv. Mater.*, 2001, **13**, 1501.

8 a) M. Shao, T. Yu, J. H. Odell, M. Jin, Y. Xia, *Chem. Commun.*, 2011, **47**, 6566; b) Y.-H. Chen, H.-H. Hung, M. H. Huang, *J. Am. Chem. Soc.*, 2009, **131**, 9114.

9 a) M. Yamauchi, R. Ikeda, H. Kitagawa, M. Takata, *J. Phys. Chem. C*, 2008, **112**, 3294; b) C. Langhammer, E. M. Larsson, B. Kasemo, I. Zorić, *Nano Lett.*, 2010, **10**, 3529.

10 a) F. Favier, E. C. Walter, M. P. Zach, T. Benter, R. M. Penner, *Science*, 2001, **293**, 2227; b) Y. Sun, H. H. Wang, *Adv. Mater.*, 2007, **19**, 2818.

11 a) Y. Xiong, B. Wiley, J. Chen, Z.-Y. Li, Y. Yin, Y. Xia, *Angew. Chem. Int. Ed.*, 2005, **44**, 7913; b) Y. Xiong, J. M. McLellan, J. Chen, Y. Yin, Z.-Y. Li, Y. Xia, *J. Am. Chem. Soc.*, 2005, **127**, 17118.

12 a) E. Antolini, *Energy Environ. Sci.*, 2009, **2**, 915; b) M. Jin, H. Zhang, Z. Xie, Y. Xia, *Angew. Chem. Int. Ed.*, 2011, **50**, 7850.

13 Y. Nishihata, J. Mizuki, T. Akao, H. Tanaka, M. Uenishi, M. Kimura, T. Okamoto, N. Hamada, *Nature*, 2002, **418**, 164.

14 a) F. Wang, C. Li, L.-D. Sun, H. Wu, T. Ming, J. Wang, J. C. Yu, C.-H. Yan, *J. Am. Chem. Soc.*, 2011, **133**, 1106; b) A. Mohanty, N. Garg, R. Jin, *Angew. Chem. Int. Ed.*, 2010, **49**, 4962.

15 M. Shao, *J. Power Sources*, 2011, **196**, 2433.

16 a) C. Bianchini, P. K. Shen, *Chem. Rev.*, 2009, **109**, 4183; b) C. Xu, P. K. Shen, Y. Liu, *J. Power Sources*, 2007, **164**, 527; c) F. Hu, C. Chen, Z. Wang, G. Wei, P. K. Shen, *Electrochim. Acta*, 2006, **52**, 1087.

17 H. Zhang, M. Jin, Y. Xiong, B. Lim, Y. Xia, *Acc. Chem. Res.*, 2013, *46*, 1783.

18 a) B. Lim, Y. Xia, *Angew. Chem. Int. Ed.*, 2011, **50**, 76; b) M. A. Mahmoud, C. E. Tabor, M. A. El-Sayed, Y. Ding, Z. L. Wang, *J. Am. Chem. Soc.*, 2008, **130**, 4590.

19 a) Z.-H. Lin, M.-H. Lin, H.-T. Chang, *Chem. Eur. J.*, 2009, **15**, 4656; b) L. Wang, M. Imura, Y. Yamauchi, *ACS Appl. Mater. Interfaces*, 2012, **4**, 2865.

20 a) Z. Yin, H. Zheng, D. Ma, X. Bao, *J. Phys. Chem. C*, 2009, **113**, 1001; b) J. Watt, S. Cheong, M. F. Toney, B. Ingham, J. Cookson, Peter T. Bishop, R. D. Tilley, *ACS Nano*, 2010, **4**, 396.

21 J. Xu, A. R. Wilson, A. R. Rathmell, J. Howe, M. Chi, B. J. Wiley, *ACS Nano*, 2011, **5**, 6119.

22 a) B. Lim, M. Jiang, T. Yu, P. H. C. Camargo, Y. Xia, *Nano Res.*, 2010, **3**, 69; b) B. Lim, M. Jiang, P. H. C. Camargo, E. C. Cho, J. Tao, X. Lu, Y. Zhu, Y. Xia, *Science*, 2009, **324**, 1302.

23 F. Ksar, G. K. Sharma, F. Audonnet, P. Beaunier, H. Remita, *Nanotechnology*, 2011, **22**, 305609.

24 Y. W. Lee, M. Kim, S. W. Han, *Chem. Commun.*, 2010, **46**, 1535.

25 D. Y. Kim, S. W. Kang, K. W. Choi, S. W. Choi, S. W. Han, S. H. Im, O O. Park, *CrystEngComm*, 2013, **15**, 7113.

26 a) X. Wang, W. Wang, Z. Qi, C. Zhao, H. Ji and Z. Zhang, *Electrochem. Commun.*, 2009, **11**, 1896; b) X. Wang, W. Wang, Z. Qi, C. Zhao, H. Ji and Z. Zhang, *Int. J. Hydrogen Energy*, 2012, **37**, 2579.

27 a) X. Peng, J. Wickham, A. P. Alivisatos, *J. Am. Chem. Soc.*, 1998, **120**, 5343; b) H. Zheng, R. K. Smith, Y. Jun, C. Kisielowski, U. Dahmen, A. P. Alivisatos, *Science*, 2009, **324**, 1309.
28 D. Kim, Y. W. Lee, S. B. Lee, S. W. Han, *Angew. Chem. Int. Ed.*, 2012, **51**, 159.
29 Z. X. Liang, T.S. Zhao, J. B. Xu, L. D. Zhu, *Electrochim. Acta*, 2009, **54**, 2203.
30 H. Wu, H. Li, Y. Zhai, X. Xu, Y. Jin, *Adv. Mater.*, 2012, **24**, 1594.
31 K. Lee, S. W. Kang, S.-U. Lee, K.-H. Park, Y. W. Lee, S. W. Han, *ACS Appl. Mater. Interfaces*, 2012, **4**, 4208.

Table of content

Chestnut-bur-like palladium nanostructures were synthesized through particle attachment growth mechanism by using CPC as a surfactant and they exhibited greater electrocatalytic activity toward ethanol oxidation reaction.

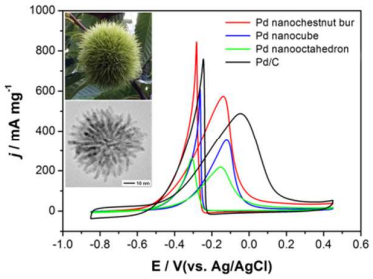

Key words

chestnut-bur-like, Pd nanostructure, morphology control, growth mechanism, catalytic activity

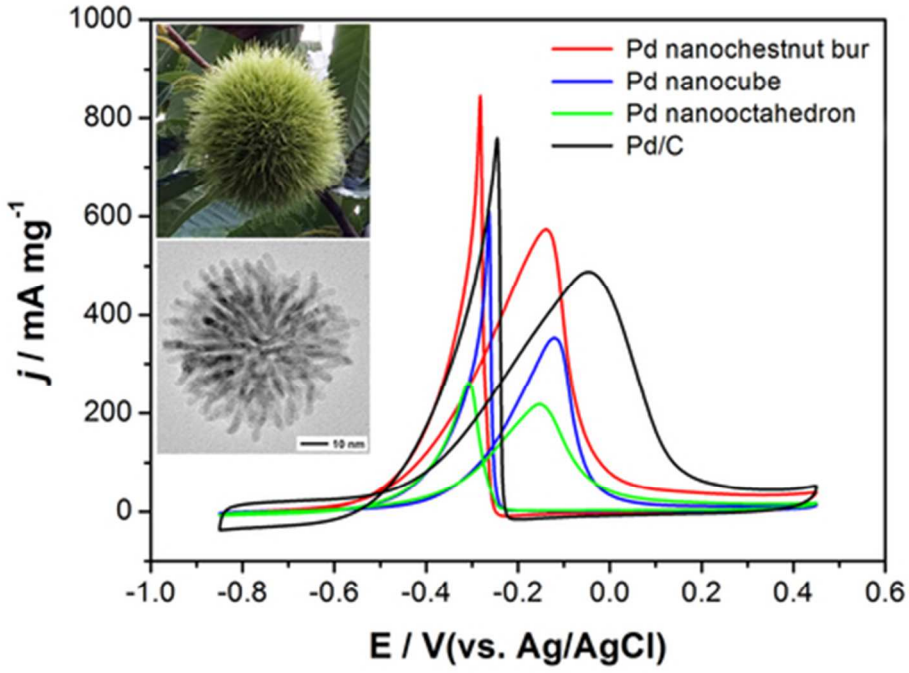

39x29mm (300 x 300 DPI)